Supplementary Information for

Diffusiophoresis promotes phase separation and transport of biomolecular condensates

Viet Sang Doan,[1] Ibraheem Alshareedah,[2] Anurag Singh,[2] Priya R. Banerjee,[2*] Sangwoo Shin[1*]

[1] Department of Mechanical and Aerospace Engineering, University at Buffalo, The State University of New York, Buffalo, NY 14260

[2] Department of Physics, University at Buffalo, The State University of New York, Buffalo, NY 14260

[*] Correspondence should be addressed to: P.R.B. (prbanerj@buffalo.edu); S.S. (sangwoos@buffalo.edu)

SUPPLEMENTARY FIGURES

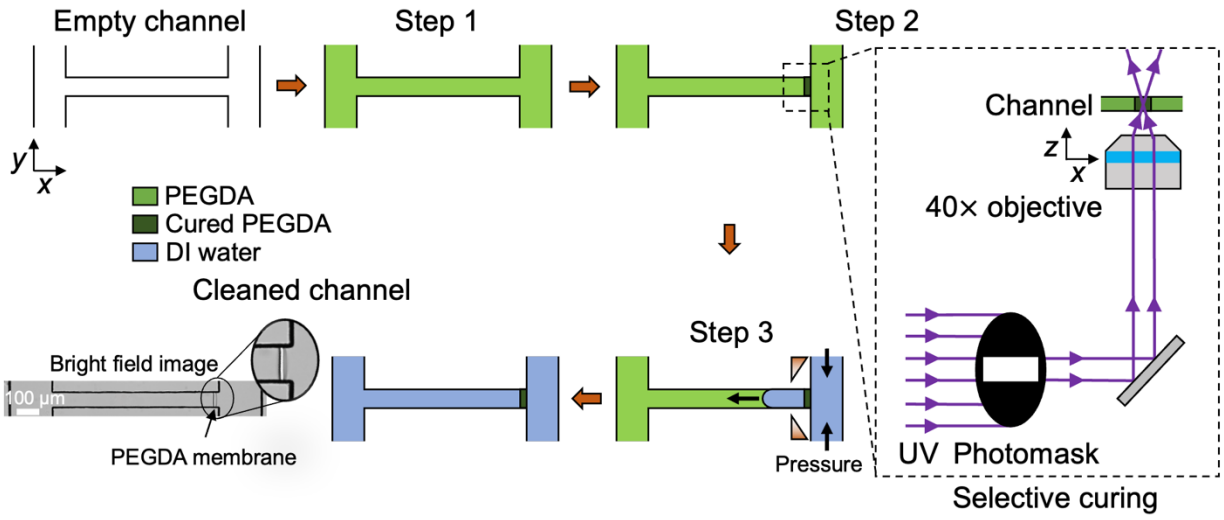

Figure S1. In situ fabrication of PEGDA membranes. In Step 1, the empty channel was filled with PEGDA solution [20% (v/v) PEGDA, 2% (v/v) photoinitiator 2-hydroxy-2-methylpropiophenone]. Then, a black mask with a thin transparent strip and 40× objective were used to selectively cure a thin region to create a PEGDA membrane (Step 2). Finally, the excessive PEGDA was flushed out through the membrane by DI water at elevated pressure (Step 3). The bright field image shows the PEGDA membrane near the right inlet of the channel.

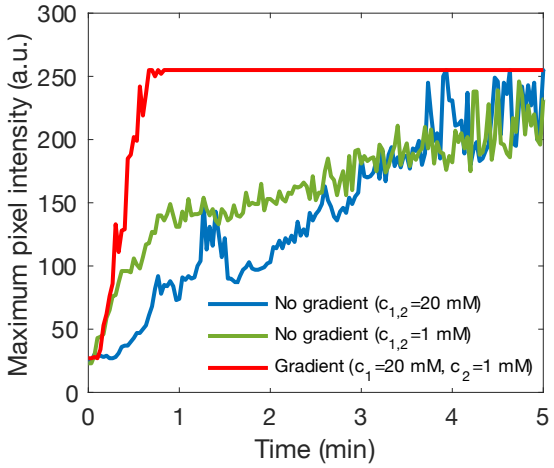

Figure S2. Local maximum fluorescence intensity of the condensates over time under different salt conditions. Data were processed from Movie S1 (Figure 1b-d). Blue, green, and red curves indicate, respectively, $c_1 = c_2 = 20$ mM (high salinity), $c_1 = c_2 = 1$ mM (low salinity), and $c_1 = 20$ mM, $c_2 = 1$ mM (NaCl gradient). The local intensity of the condensates under diffusiophoresis becomes quickly saturated to the maximum value (intensity = 255), while the fluorescence intensities of the condensates in the absence of salt gradients were far below the saturation, indicating enhanced phase separation by diffusiophoresis. Source data are provided as a Source Data file.

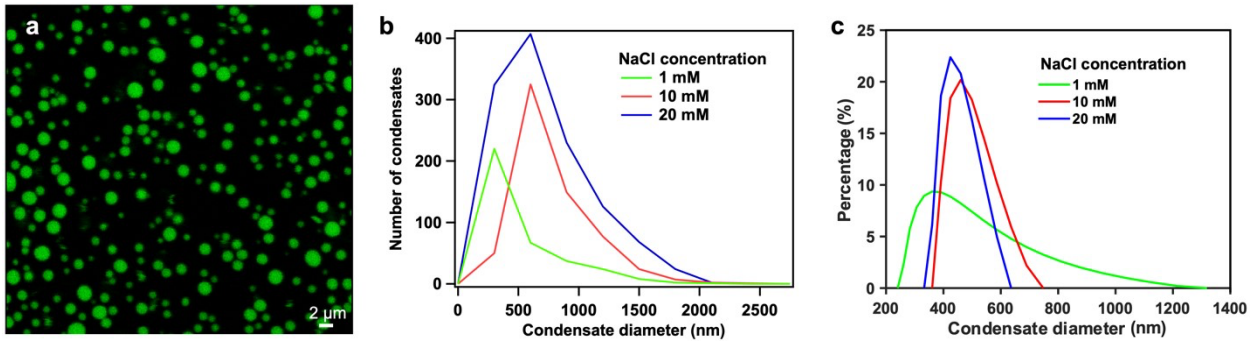

Figure S3. Size distribution of $[dT]_{40}$-$[RGRGG]_5$ condensates ($[dT]_{40}$:$[RGRGG]_5$ = 1.25:1). (**a**) Confocal image of $[dT]_{40}$-$[RGRGG]_5$ condensates in 20 mM NaCl (sample composition: 0.5 mg/ml $[RGRGG]_5$, 150 nM Alexa-488 labeled $[RGRGG]_5$, 0.625 mg/ml $[dT]_{40}$, 10 mM Tris-HCl, 20 mM DTT, and 20 mM NaCl). (**b**, **c**) Size distribution of $[dT]_{40}$-$[RGRGG]_5$ condensates at varying NaCl concentrations obtained from the (**b**) confocal imaging and (**c**) dynamic light scattering. Source data are provided as a Source Data file.

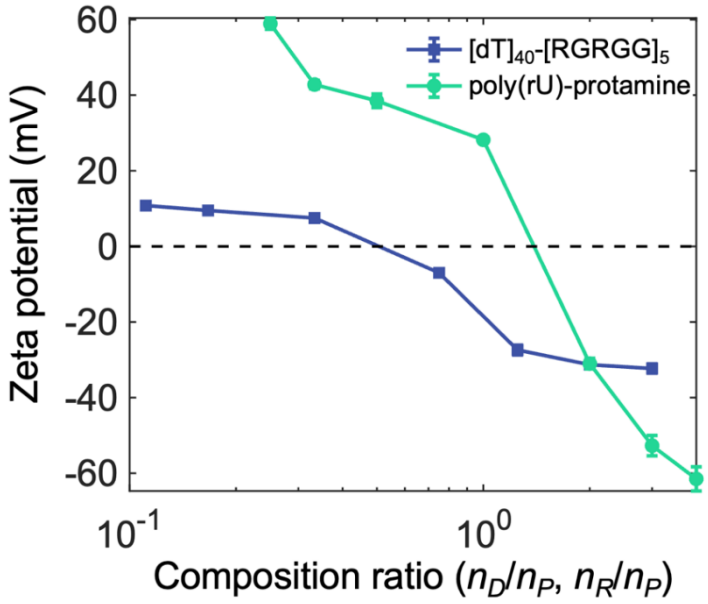

Figure S4. Zeta potential of [dT]$_{40}$-[RGRGG]$_5$ and poly(rU)-protamine complexes with varying composition ratios (ssDNA/RNA-to-protein; $n_{\{D,R\}}/n_P$) in 10 mM Tris-HCl and 10 mM NaCl. Error bars represent standard deviation. Source data are provided as a Source Data file.

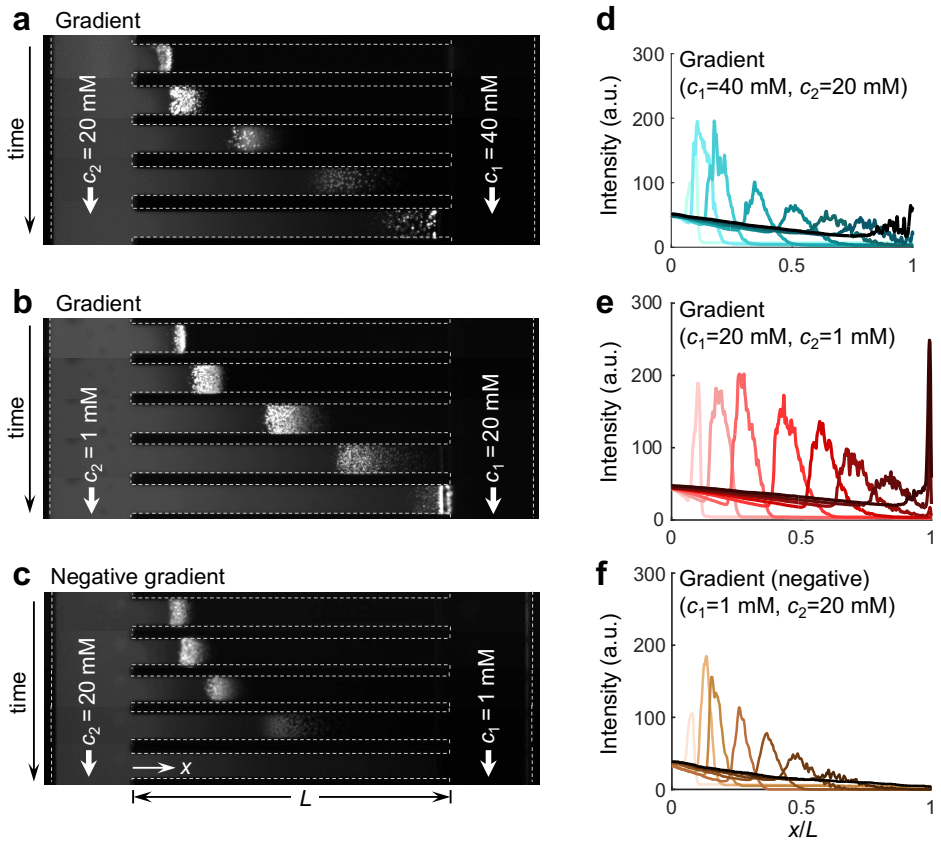

Figure S5. Formation and transport of the condensates under different salt conditions. (**a-c**) The image sequences and (**d-f**) their corresponding width-averaged intensity distribution of the formation and transport $[dT]_{40}$-$[RGRGG]_5$ condensates over 60 minutes. The NaCl concentrations are (**a,d**) c_1 = 40 mM, c_2 = 20 mM, (**b,e**) c_1 = 20 mM, c_2 = 1 mM, and (**c,f**) c_1 = 1 mM, c_2 = 20 mM. For (**a**) and (**b**), the concentration difference is nearly identical in both cases (~20 mM). However, the formation and transport of the condensates in (**b**) are stronger than in (**a**) due to the logarithmic dependence of diffusiophoresis. In (**c**), the concentration gradient is imposed in the reverse direction compared to (**b**), showing weaker phase separation and wave motion. The timestamps for the images in (**a-c**) are 1, 5, 20, 40, and 60 min, and for the plots in (**d-f**) are 1, 5, 10, 20, 30, 40, 50, and 60 min. Source data are provided as a Source Data file.

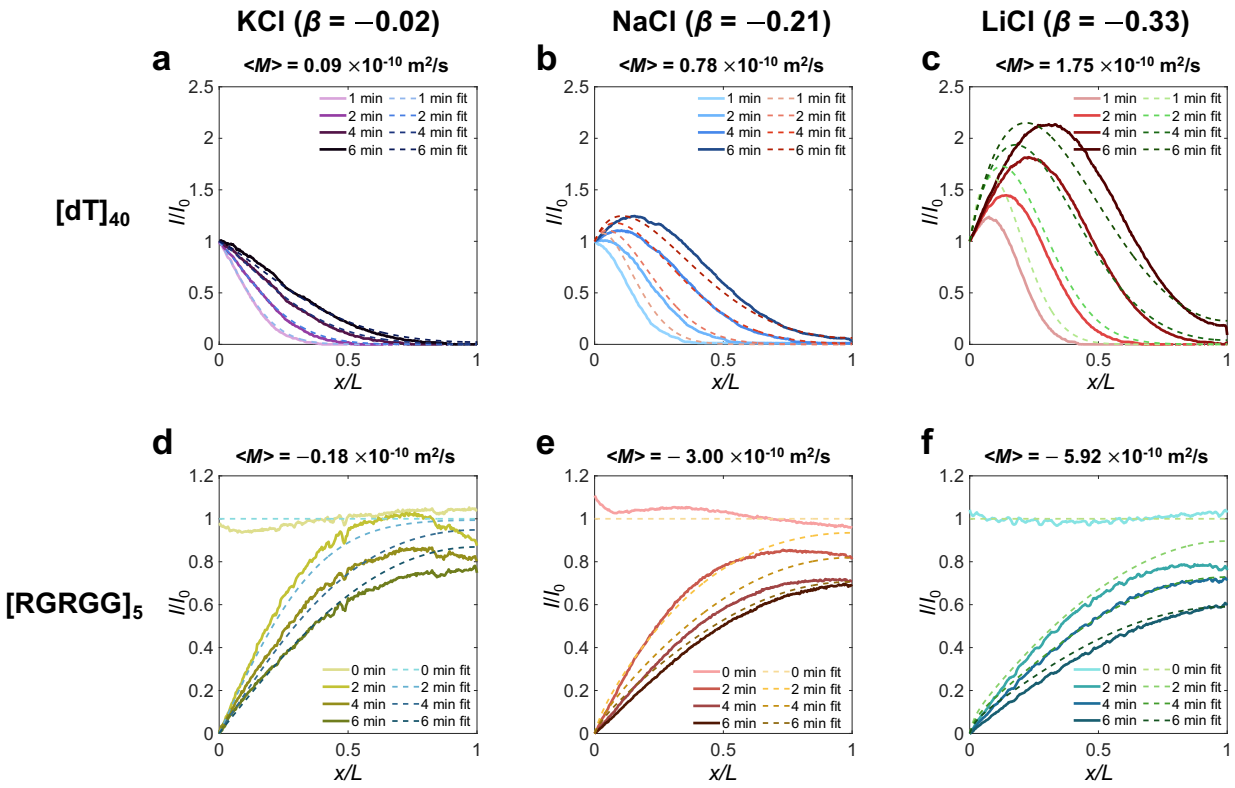

Figure S6. The diffusiophoretic mobility of $[dT]_{40}$ and $[RGRGG]_5$ in various types of salts (varying β). (**a-c**) The mobility of $[dT]_{40}$ and (**d-f**) $[RGRGG]_5$ in KCl, NaCl, and LiCl gradient, respectively. The highest mobilities were observed in LiCl (**c,f**), while the values were the lowest in the KCl gradient (**a,d**). These differences in mobilities across different salts suggest that the transport of $[dT]_{40}$ and $[RGRGG]_5$ is influenced by diffusiophoresis, which is dependent on the diffusivity contrast between ions resulting from the varying salt gradients. Source data are provided as a Source Data file.

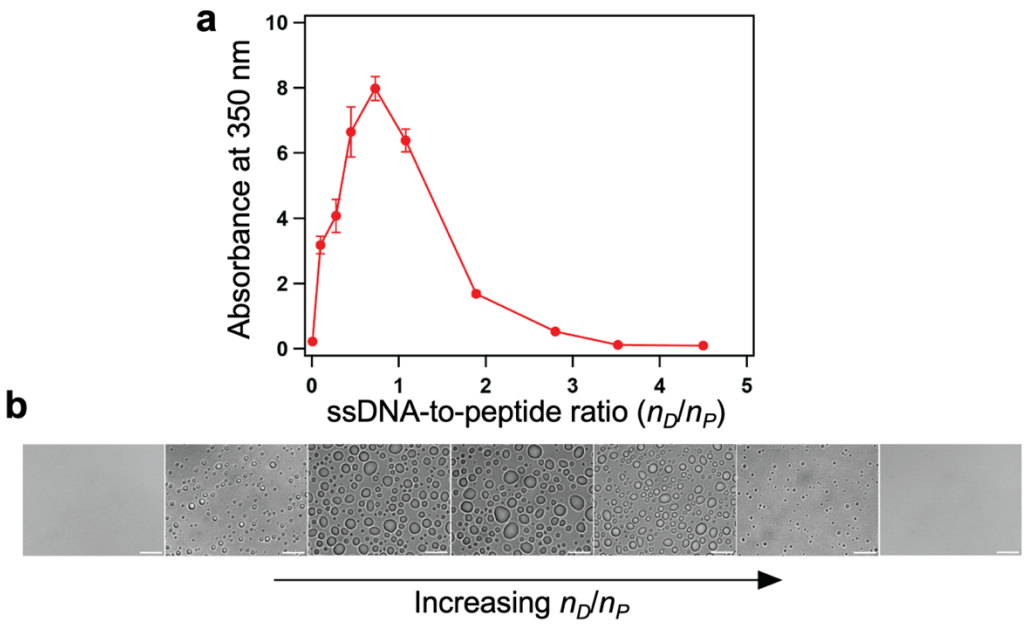

Figure S7. (**a**) A plot showing absorbance at 350 nm (turbidity) of $[dT]_{40}$-$[RGRGG]_5$ mixtures at different mixing stoichiometries. Error bars represent standard deviation. (**b**) Brightfield images of the condensates formed at increasing ssDNA-peptide selected mixing ratios for which turbidity measurements were performed in (**a**). The scale bar is 10 µm. From both (**a**) and (**b**) reentrant phase separation of $[dT]_{40}$-$[RGRGG]_5$ condensates is evident. Source data are provided as a Source Data file.

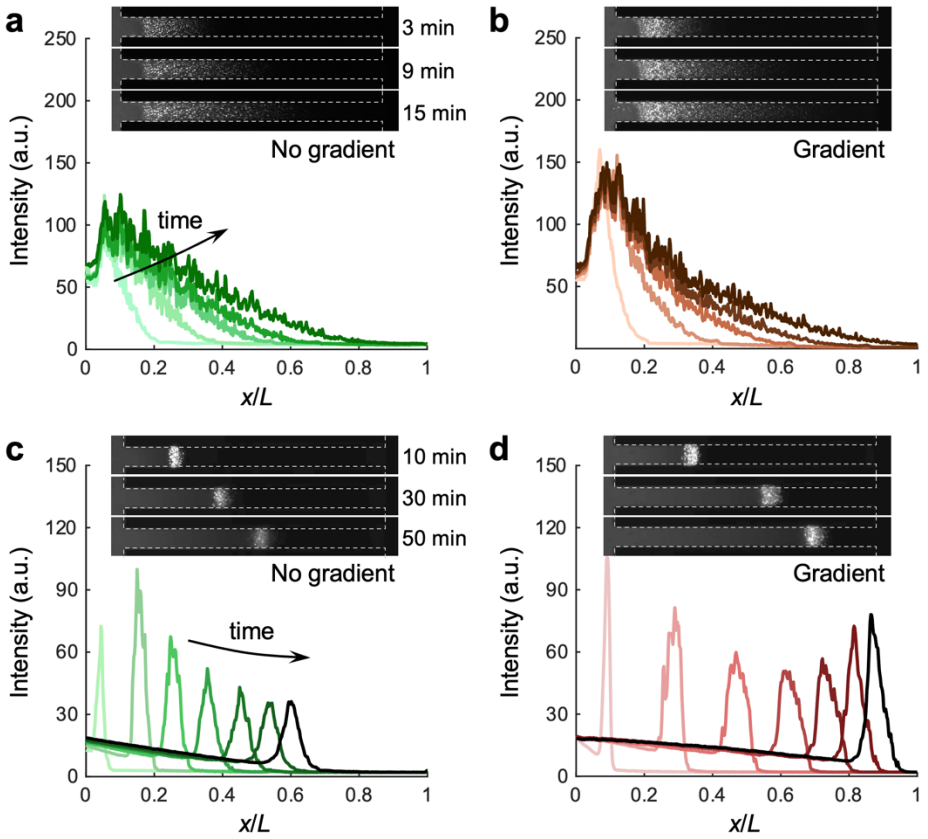

Figure S8. Fluorescence images of (**a,b**) $[RGRGG]_5$-rich $[dT]_{40}$-$[RGRGG]_5$ condensates (**a**) without (c_1 = c_2 = 20 mM) or (**b**) with KAc gradients (c_1 = 20 mM and c_2 = 1 mM), and (**c,d**) poly(rU)-rich poly(rU)-protamine condensates (**c**) without (c_1 = c_2 = 20 mM) or (**b**) with NaCl gradients (c_1 = 20 mM and c_2 = 1 mM). The timestamps for the intensity profiles for (**a,b**) are 1, 3, 6, 9, and 15 min, and (**c,d**) are 1, 10, 20, 30, 40, 50, and 60 min, respectively. Source data are provided as a Source Data file.

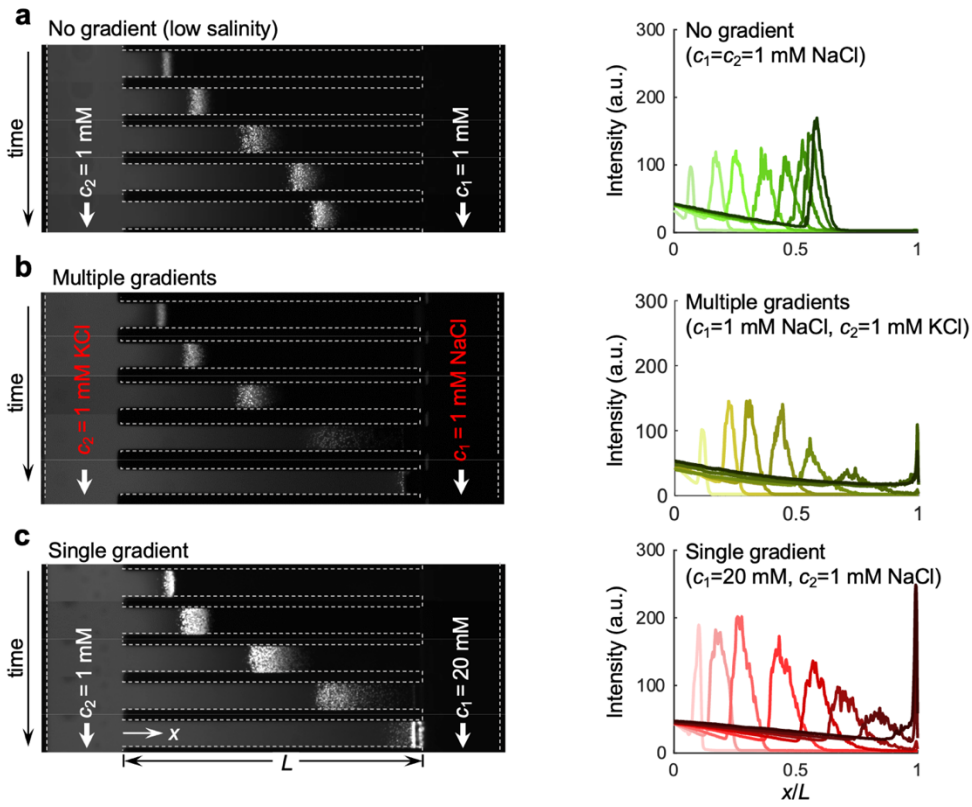

Figure S9. Formation and transport of condensates by interdiffusion of equimolar multispecies solutes. (**a**) The image sequences the formation and transport of $[dT]_{40}$-$[RGRGG]_5$ condensates over a 60-minute period (**a**) without any salt gradient ($c_1 = c_2$ = 10 mM NaCl); (**b**) under interdiffusion of equimolar NaCl and KCl (c_1 = 1 mM NaCl, c_2 = 1 mM KCl) and (**c**) under NaCl gradient (c_1 = 20 mM, c_2 = 1 mM). In the case of interdiffusion of equimolar NaCl and KCl in (**b**), due to the difference in the diffusion coefficients of Na^+ and K^+, a local electrical field arises, causing electrophoresis. As a result, the transport and the formation of the condensate are improved compared to the case of no salt gradients (**a**). However, the lack of chemiphoresis in (**b**) due to the equimolar concentration leads to relatively weaker improvement in the transport and formation compared to the single NaCl gradient case in (**c**). Source data are provided as a Source Data file.

SUPPLEMENTARY DISCUSSION

Diffusiophoresis in $[RGRGG]_5$-rich and poly(rU)-rich condensates

We have investigated the salt gradient effects in other biomolecular systems, e.g., different stoichiometry or species. For instance, we studied $[RGRGG]_5$-rich $[dT]_{40}$-$[RGRGG]_5$ condensates by introducing $[RGRGG]_5$ at an elevated concentration of 0.9 mg/ml in the left reservoir while lowering the concentration of $[dT]_{40}$ to 0.15 mg/ml in the center and right channels (**Supplementary Figs. S8a,b**). Because of the opposite configuration, we choose potassium acetate (KAc) as the solute, which can drive $[RGRGG]_5$ up the gradient and $[dT]_{40}$ down the gradient due to the positive β factor ($\beta = 0.29$) such that diffusiophoresis is expected to accelerate their migration toward each other. We observe that the KAc gradients ($c_1 = 20$ mM, $c_2 = 1$ mM) resulted in a stronger condensate formation, but did not significantly affect the transport of the formed condensates (**Supplementary Figs. S8a,b**). This is because KAc gradients can accelerate the transport of individual $[RGRGG]_5$ and $[dT]_{40}$ molecules (**Supplementary Fig. S5**), thus a more robust condensate formation is expected. However, the condensates do not experience any significant active motility due to the low zeta potential ($\zeta = 9.5$ mV; **Supplementary Fig. S4**) of $[RGRGG]_5$-rich condensates. We note that $[dT]_{40}$-$[RGRGG]_5$ mixtures display an asymmetric charge inversion behavior (**Supplementary Fig. S4**) where the $[dT]_{40}$-rich condensates carry more charge than the $[RGRGG]_5$-rich condensates, similar to previously reported poly(rU)-$[RP]_3$ system,[1] and poly(rA)-$[RGRGG]_5$ condensates.[2]

The poly(rU)-protamine condensates were formed by introducing poly(rU) in the left reservoir (1.2 mg/ml) and protamine initially in the center and right channels (0.3 mg/ml). Using NaCl, we observe similar behavior to $[dT]_{40}$-rich $[dT]_{40}$-$[RGRGG]_5$ condensates, where the negatively charged condensates were formed and the transport of poly(rU)-protamine condensates was improved under NaCl gradients ($c_1 = 20$ mM and $c_2 = 1$ mM) (**Fig. S8c**) in comparison with the case without NaCl gradient ($c_1 = c_2 = 20$ mM; **Fig. S8d**). This is due to the high negative surface charge ($\zeta = -61.5$ mV at RNA-to-protein ratio 4; **Fig. S4**) of the poly(rU)-rich condensates.

SUPPLEMENTARY REFERENCES

1. Banerjee, P. R., Milin, A. N., Moosa, M. M., Onuchic, P. L. & Deniz, A. A. Reentrant Phase Transition Drives Dynamic Substructure Formation in Ribonucleoprotein Droplets. *Angew. Chem. Int. Ed.* **56**, 11354–11359 (2017).
2. Alshareedah, I. *et al.* Interplay between Short-Range Attraction and Long-Range Repulsion Controls Reentrant Liquid Condensation of Ribonucleoprotein–RNA Complexes. *J. Am. Chem. Soc.* **141**, 14593–14602 (2019).